Direct measurement of the lamellipodial protrusive force in a migrating cell

Marcus Prass,[1] Ken Jacobson,[2,3] Alex Mogilner,[4,5] and Manfred Radmacher[1]

[1]Institute of Biophysics, University of Bremen, D-28359 Bremen, Germany
[2]Department of Cell and Developmental Biology and [3]Lineberger Comprehensive Cancer Center, University of North Carolina at Chapel Hill, Chapel Hill, NC 27599
[4]Department of Mathematics and [5]Center for Genetics and Development, University of California, Davis, Davis, CA 95616

There has been a great deal of interest in the mechanism of lamellipodial protrusion (Pollard, T., and G. Borisy. 2003. *Cell*. 112:453–465). However, one of this mechanism's endpoints, the force of protrusion, has never been directly measured. We place an atomic force microscopy cantilever in the path of a migrating keratocyte. The deflection of the cantilever, which occurs over a period of ~10 s, provides a direct measure of the force exerted by the lamellipodial leading edge. Stall forces are consistent with ~100 polymerizing actin filaments per micrometer of the leading edge, each working as an elastic Brownian ratchet and generating a force of several piconewtons. However, the force-velocity curves obtained from this measurement, in which velocity drops sharply under very small loads, is not sensitive to low loading forces, and finally stalls rapidly at large loads, are not consistent with current theoretical models for the actin polymerization force. Rather, the curves indicate that the protrusive force generation is a complex multiphase process involving actin and adhesion dynamics.

Introduction

Elucidation of the detailed mechanisms of how cells move has been of increasing interest (Lauffenburger and Horwitz, 1996; Pollard and Borisy, 2003; Ridley et al., 2003). Much attention has been focused on the molecular mechanism of the first step of this movement, protrusion and its regulation (Small et al., 2002; Pollard and Borisy, 2003). Far fewer efforts have dealt with how the molecular mechanisms actually produce protrusive force (Condeelis, 1993; Bray, 2001), and even fewer make a quantitative prediction of what the protrusive force should be (Mogilner and Oster, 1996, 2003; Carlsson, 2003; Dickinson et al., 2004). Despite earlier attempts to measure lamellar stiffness using microneedles (Felder and Elson, 1990) and recent attempts to ascertain the lamellar protrusive force indirectly (Ladam et al., 2005; Bohnet et al., 2006), it has never been measured directly. The goal of this study was to measure the maximum (stall) force the lamellipod could produce and the characteristic force-velocity relation for the lamellipod. Such information would be invaluable in evaluating quantitative models for protrusive force production by the lamella of migrating cells. The concept was to place a flexible barrier of known stiffness in front of a portion of the leading edge of a migrating cell. Deflection of the barrier by the moving cell would apply a load force to that portion of the advancing lamellipod. The lamellipod will apply an equal and opposite protrusive force to the barrier, and, as the load force increases, the lamellipod velocity will decrease eventually to zero when the leading edge stalls. At this point, the maximum possible protrusive force will be exerted by the cell against the load.

Correspondence to Manfred Radmacher: mr@biophysik.uni-bremen.de

Abbreviations used in this paper: AFM, atomic force microscopy; RICM, reflection interference contrast microscopy.

The online version of this article contains supplemental material.

Results and discussion

To experimentally implement this concept, we fabricated a microscope stage that permits the positioning of a soft SiN atomic force microscopy (AFM) cantilever in the path of a migrating fish keratocyte (Fig. 1, a and b). Particularly critical is the height adjustment: it must block the thin lamellipod without touching the substrate, which would produce a stall that occurs too quickly because of the lamella pushing a cantilever that is not free. The pyramidal tip of the cantilever, which is normally for scanning the sample, could be imaged (Fig. 1 c), and its position could be measured to subpixel accuracy as the cell deflected it. Fig. 1 c (also see Video 1, available at http://www.jcb.org/cgi/content/full/jcb.200601159/DC1) shows selected frames from the entire time course of the experiment, from initial contact with the edge at t = 0 to deformation of the lamella at t = 30 s, contact with the nuclear mound at 60 s, maximal deflection of the cantilever at 233 s, and ending with release of the cantilever

The Journal of Cell Biology, Vol. 174, No. 6, September 11, 2006 767–772
http://www.jcb.org/cgi/doi/10.1083/jcb.200601159

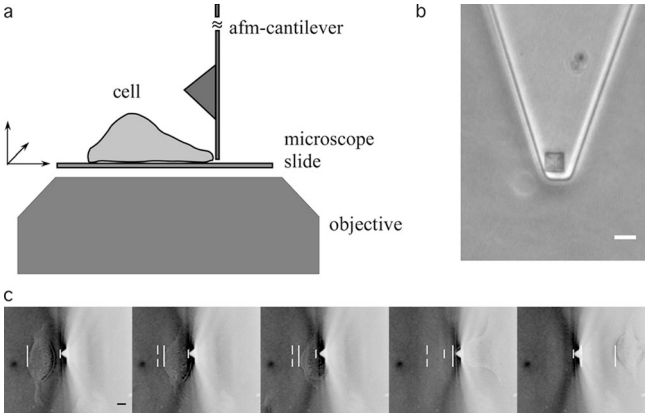

Figure 1. **Experimental setup.** (a) Schematic diagram showing the position of the cantilever with respect to the oncoming cell. (b) Micrograph of the base of a cantilever, indicating the region of contact with the lamellipod (see supplemental material). (c) Series of images of direct force measurement at t = 0, 30, 60, 233, and 260 s, from left to right. Small white line, initial position of the cantilever; large white line, current dorsal part of the cell; dashed white line, large white line from the previous image. Bars, 5 μm. Also see Video 1 (available at http://www.jcb.org/cgi/content/full/jcb.200601159/DC1).

after the cell moves on (Video 1, frame at 260 s). Knowing the stiffness of the cantilever and measuring its deflection (see Materials and methods) permits the load force to be calculated by Hooke's Law as the cell moves against the cantilever (Fig. 2 a). The load force increases with time until a stall of the entire cell occurs, after which the cell escapes and the load force drops abruptly to zero. The whole cell stall force (stalling the forward translocation of the cell body rather than blocking the lamellipodial leading edge protrusion) is ∼40 nN, which is consistent with previous results on keratocytes using calibrated microneedles (Oliver et al., 1995).

One of the features in Fig. 2 a is the period of initial contact, which is highlighted. This section is expanded in Fig. 2 b. The initial contact of the lamellipod is followed by a rapid increase in load force as the lamellipod pushes the cantilever, eventually stalling after 6–8 s (Fig. 2 b, highlighted section). One issue was whether a portion of the lamellipod adjacent to the substrate actually slipped under the cantilever as opposed to the cantilever blocking the lamellipod as desired. We investigated this by rapid fixation shortly after the cantilever struck the leading edge of the cells using a protocol described by Lee and Jacobson (1997). Such a cell is seen in Fig. 2 c stained for filamentous actin by rhodamine-phalloidin. Contact-mode AFM of the same fixed cell (Fig. 2 d) demonstrates that no part of the lamellipod slipped under the cantilever, as bare substratum can be seen where the cantilever indented the leading edge. (It should be noted that the indentation at that time is much larger than the indentations when the protrusion force is measured in the first 10 s after cantilever contact; such indentations are more difficult to visualize). This suggests that the lamellipod behaves as an integral unit consistent with its inherent stiffness (Felder and Elson, 1990). In addition, the region at the base of the indentation, which actually has closed somewhat by the time fixation has occurred, does not appear to be appreciably higher. The typical height of the lamellipod of a keratocyte is only ∼140–200 nm (Laurent et al., 2005). This corroborates the assertion that the contact length of the cantilever where it hits the lamellipod will be ∼3 μm; this is the long dimension of the cantilever at its base (Fig. 1 b).

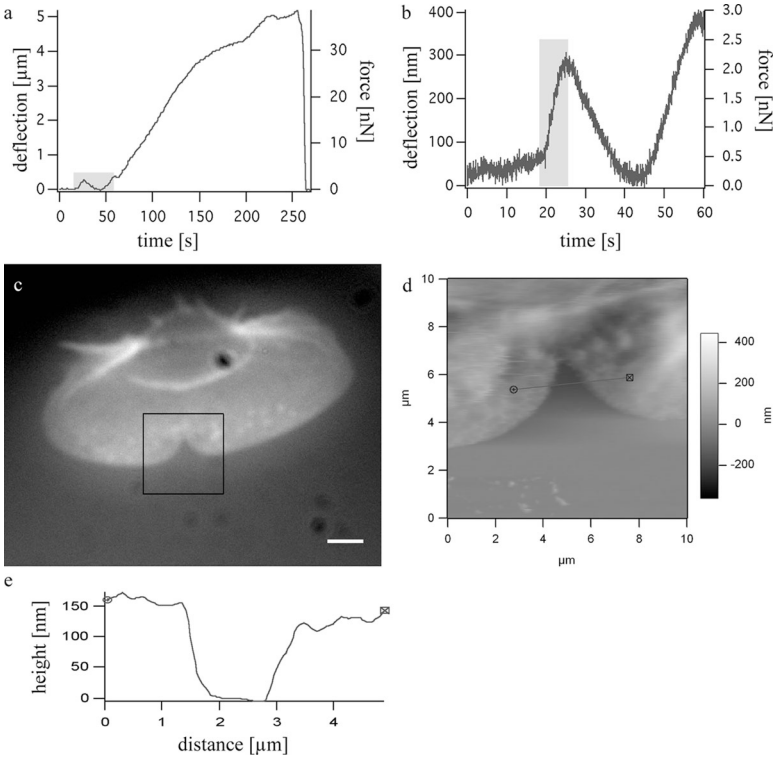

Figure 2. **Stall experiments of migrating keratocytes.** (a) Deflection/force versus time for a whole cell. (b) Highlighted region from panel a representing deflection by the lamellipod. (c–e) Effects of cantilever impinging on the leading edge of a trout keratocyte followed by withdrawal of the cantilever and immediate fixation (see Materials and methods). (c) Rhodamine-phalloidin labeling of filamentous actin, with indentation caused by the cantilever. Boxed area is shown in panel d. Bar, 5 μm. (d) Same region of the lamellipod imaged by contact-mode AFM. (e) Height profile along the line in panel d.

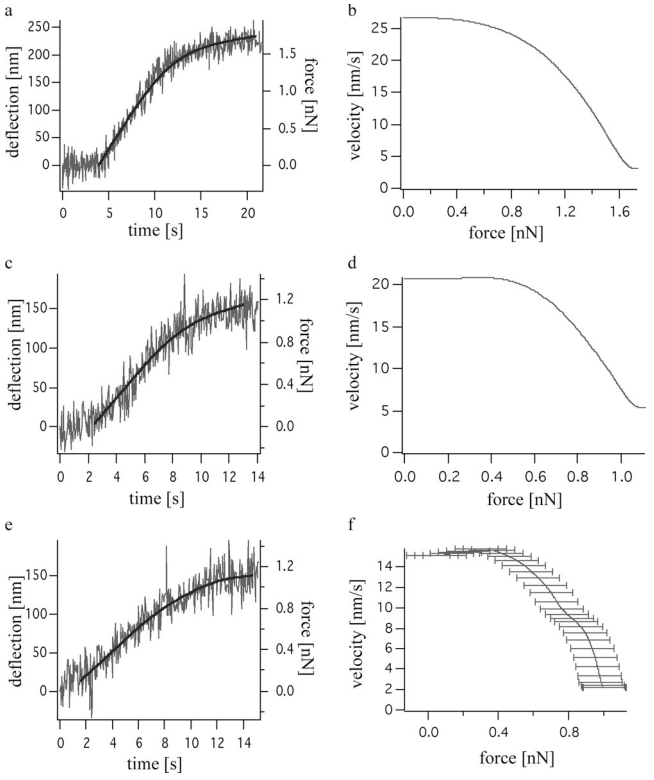

Figure 3. **Three representative deflection/force versus time curves and corresponding force-velocity curves.** (a, c, and e) Deflection/force versus time curves for the lamellipod hitting the cantilever. (b, d, and f) Corresponding force-velocity curves for each example on the left. Representative error bars were calculated as described in Materials and methods for every 10th data point.

Note that after the leading edge is stalled locally, the parts of the leading edge adjacent to the stalled region continue to advance and deform, and, on the scale of tens of seconds, the lamellipodial actin network undergoes significant remodeling so that the lamellipod "sneaks around" the cantilever. In ~20 s, the cantilever hits the mound of the cell body and starts to deflect significantly (Fig. 2 and Video 2, available at http://www.jcb.org/cgi/content/full/jcb.200601159/DC1).

Three representative examples of the force versus time curves are given in Fig. 3 (a, c, and e). Because the cantilever is assumed to maintain contact with the protruding lamellipod, differentiating the position of the cantilever as a function of time gives the velocity of that portion of the lamellipod. This enables force-velocity relations to be plotted for each force-time curve as shown in Fig. 3 (b, d, and f). The mean stall force (where the cantilever movements stops, at least momentarily) is 1.18 ± 0.35 nN (SD; $n = 12$). Table I shows the variability in individual cells regarding stall force, initial cantilever velocity at the point where it contacts the cell, and velocity of the trailing edge of the cell at the moment the cantilever contacts the leading edge. These two velocities are uncorrelated, and neither of them is correlated with the stall force.

A surprising element of this study was that the initial cantilever velocity, rather than being equal to the cell body forward translocation rate, was considerably (by about a factor of seven) reduced (Table I), indicating that the protrusion rate decreases

Table I. **Aggregate single-cell data**

Cell No.	V_{max}	V0	F_{max}	$V0/V_{max}$
	nm/s	*nm/s*	*nN*	
1	57	167	1.54	2.9
2	16	223	1.13	13.9
3[a]	9	327	0.5	36
4	20	144	0.89	7.2
5	18	60	1.02	3.3
6	18	123	1.21	6.8
7	15	204	1.01	13.6
8	21	145	1.12	6.9
9	18	71	1.05	3.9
10	27	135	1.74	5
11	27	162	1.83	6
12	28	186	0.98	6.6
13	16	117	0.65	7.3

V_{max}, maximal velocity of the cantilever at the moment of contact with the cell. V0, maximal velocity of the cell measured at the trailing edge approximately when the cantilever contacts the cell. F_{max}, stall force.
[a]This cell was rejected from the calculation because of obvious discrepancies, but it is shown to demonstrate the variations of the values.

abruptly upon contact. Mechanically speaking, this decrease could be caused by initial contact and loading not visible to us (forces of the order of ≤100 pN would cause deflections so small that they would be undetectable from the images). Chemically speaking, signaling material that accumulated on the cantilever does not appear to be a factor, as the velocity reduction effect is seen with both clean cantilevers and those used multiple times. Rather, the leading edge of the cell appears to slow down just before or at the initial instant of striking the cantilever. To ask when this reduction in lamellipodial velocity occurred, we used reflection interference contrast microscopy (RICM) in which close adhesions at the cell ventral surface and the cantilever as a stationary obstacle could be simultaneously visualized. To avoid pronounced reflections from the gold-coated cantilever, which obscures events when the cantilever is in close proximity to the leading edge, we used uncoated SiN cantilevers. This setup enabled us to observe that lamellipod slowdown occurs within typically ≤2 pixels (corresponding to 232 nm; $n = 12$) in front of the cantilever (Fig. 4 and Video 2). If there is a narrow nonadherent rim of the leading edge that extends beyond the most anterior close contacts visualized by RICM (Lee and Jacobson, 1997), slowdown occurs even closer to the cantilever. At this juncture, we favor the idea that the cell mechanically senses the presence of the proximate cantilever and tunes the protrusion velocity and force generation mechanism accordingly (see the last two paragraphs of this section). However, remote sensing by the cell of chemical/electrochemical gradients on the tens of nanometer–length scale cannot be absolutely ruled out.

Our provisional interpretation of the stall forces is as follows. If we assume that the 3-μm region of the lamellipod edge in contact with the cantilever is stalled independently of the rest of the lamellipodial edge and that ~4 pN of force is generated per filament (the elastic Brownian ratchet model predicts ~2–7 pN per filament; Mogilner and Oster, 1996), there must be ~100 active filaments impinging on 1 μm of the leading edge.

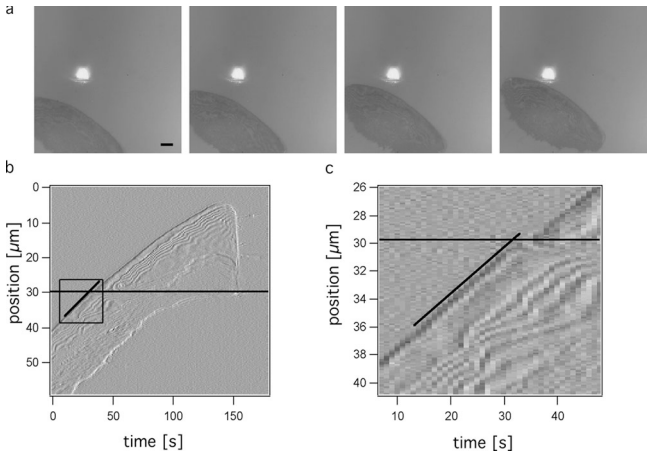

Figure 4. **Lamellipod slowdown occurs within 250 nm of the cantilever.** (a) Time series of RICM images from an RICM video as the keratocyte approaches a stationary, uncoated SiN cantilever (see Video 2, available at http://www.jcb.org/cgi/content/full/jcb.200601159/DC1). Bar, 5 μm. The temporal difference between the images is 10 s. (b) Kymograph describing the position of the lamellipod edge as a function of time as it approaches the cantilever. From each image of a video sequence of 180 frames (at 1 frame/s), the same vertical line was selected that captures contact between the cell and cantilever. To better detect the edge, the spatial derivative along the line was calculated. Such lines from successive images formed the kymograph. (c) Boxed region in panel b at a higher magnification. The horizontal lines in panels b and c indicate the position of the cantilever, whereas the diagonal lines show the movement of the edge of the cell toward the cantilever.

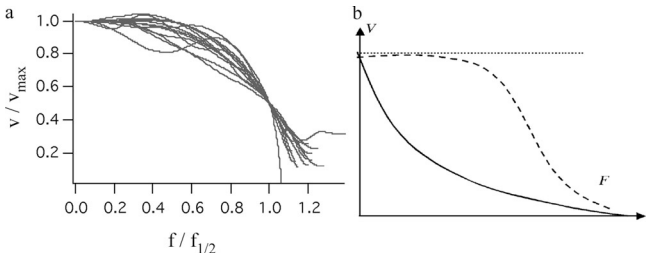

Figure 5. **Experimental data and theoretical prediction of different models.** (a) Normalized force-velocity relation. (b) Force-velocity relations predicted by the ratchet model (solid line), hypothetical stepping motor model (dashed line), and autocatalytic branching model (dotted line).

For comparison, V. Small estimates ∼120 filaments per micrometer from electron micrographs of the trout keratocyte leading edge (Small, V., personal communication). Abraham et al. (1999) have estimated the number of actin filaments in the fibroblast lamellipod to be ∼240 in a frontal area of 176 nm × 1 μm. If we assume that the area in contact with the cantilever is ∼200 nm × 3 μm, effective pressures caused by the actin polymerization at stall can be calculated. For keratocytes, the lamellipodial pressure is ∼2 nN/μm^2 (2 kPa), whereas for fibroblasts, it is ∼10 nN/μm^2 (10 kPa; Abraham et al., 1999). In comparison, the measured polymerization pressure for an actin comet tail modeling that in *Listeria monocytogenes* is ∼1 nN/μm^2 (1 kPa; Marcy et al., 2004; Parekh et al., 2005).

Fig. 5 a shows force-velocity relationships normalized by the unloaded velocity and the stall force. (Note that the initial sharp drop of velocity at forces of the order of ≤100 pN is not depicted). They indicate that at low force, the velocity is insensitive to the load, whereas at high loads, the velocity of the lamellipod decreases sharply similar in form to the recent measurement for in vitro *L. monocytogenes*–like actin networks (Parekh et al., 2005). The initial force-insensitive region is not caused by a geometric effect of a flat cantilever hitting a curved leading edge (the estimate in supplemental material shows that it would take only a second or so for the part of the cell not initially tangent to the cantilever to hit it, whereas the flat part of the force-velocity curve persists for 5–8 s; available at http://www.jcb.org/cgi/content/full/jcb.200601159/DC1).

Interestingly, the force-velocity relation we measured conforms neither to recent theoretical models (Fig. 5 b) nor to a previously measured force-velocity relation of actin comet tails. Marcy et al. (2004) and McGrath et al. (2003) obtained a convex (bending up) force-velocity relation in which the velocity decreases rapidly at low loads and slowly decreases at a greater force, which is in sharp contrast to our measurement. Only Parekh et al. (2005) observed a concave (bending down) force-velocity relation; however, in contrast with our data, their velocity increased before it became insensitive to the load, possibly as a result of transient actin growth effects. The elastic polymerization ratchet (Mogilner and Oster, 1996, 2003) as well as the elastic propulsion theory (Marcy et al., 2004) also predicts a convex force-velocity relation. The theory of autocatalytic branching (Carlsson, 2003) predicts a constant protrusion rate that is completely insensitive to force (Fig. 5) because greater load indirectly increases the Arp2/3-mediated branching and effective density increase of the actin network. Curiously, in vitro, such a force-velocity relation was measured for a bead undergoing actin-based motility in a purified protein system (Wiesner et al., 2003), albeit for small forces that we cannot probe. The filament end–tracking motor model (Dickinson et al., 2004) assumes the existence of a motorlike molecular complex at the filamentous actin barbed end and predicts a few possible force-velocity relations, one of which is concave (bending down; Fig. 5). None of the existing theories predicts the observed complex three-phase force-velocity relation: a sharp drop of velocity at a very small load, a region where velocity is insensitive to low loads, and an abrupt decrease of velocity at large loads and subsequent stall.

There are several theoretical possibilities that could explain the observed force-velocity relation. The initial sharp drop of velocity at very small forces of tens of piconewtons per micrometer can be explained in the following ways: (1) weak adhesions at the leading edge that limit the polymerization rate and either slide (Jurado et al., 2005) or stop to assemble (Bohnet et al., 2006) at very small loads; (2) small osmotic/hydrostatic pressure at the leading edge (Charras et al., 2005); or (3) thermal membrane undulations that can be dampened by small loads (Mogilner and Oster, 1996). In principle, the first sharp drop of velocity could be explained by rapid recoil of the softer lamellipodial network when it encounters the stiffer cantilever. If this is the case, this part of the force-velocity relation is not a feature of the lamellipodial network but rather is a result of the measurement technique. These possibilities are discussed in detail in the supplemental material.

The insensitivity of the velocity to low loads and its sharp drop at a greater load can be the result of a few possibilities. (1) This could be the result of two sequential processes, one of which is force independent (for example, the chemical reactions associated with adhesion). In that case, at small loads, the force-limited process is much faster than the force-independent process, and the average duration of the step of protrusion is force independent. However, at a greater load, the force-limited process becomes slower than the force-independent one, and the average duration of the step of protrusion increases with the load. Several molecular motors (for example, RNA polymerase [Wang et al., 1998] and kinesin [Schnitzer et al., 2000]) and possibly myosin VI (Iwaki et al., 2006) have such force-velocity relations for this reason. (2) Another possibility is that a strong local osmotic/hydrostatic pressure (Charras et al., 2005) or gel swelling pressure (Herant et al., 2003) is the force-generating mechanism at the leading edge, in which case the velocity would not depend on the load until the pressure at the leading edge is overcome, and then actin polymerization is rapidly stalled, leading to a concave force-velocity relation. (3) Yet another possibility is the force-dependent reinforcement of the dendritic actin network by accelerated branching (Carlsson, 2003). (4) Finally, the elastic ratchet model can explain the concave force-velocity curve if actin filaments at the leading edge are short and rigid (Mogilner and Oster, 1996). To summarize, the stall force we measure agrees well with the elastic polymerization ratchet model, but the measured convex force-velocity relation poses a challenge to models of protrusion.

In vivo, the force-velocity curve, which was measured with an AFM cantilever as described above, results from an interdependent composite of multiple, possibly redundant mechanisms and limiting factors, including actin polymerization, local osmotic pressure, molecular motors, adhesion, and viscoelastic coupling to regions proximate to the cantilever, rather than a single process such as actin polymerization that can be isolated in in vitro systems (Marcy et al., 2004; Parekh et al., 2005). (This interdependence of factors can be seen by the fact that a weak shear flow of only ~0.01 nN/μm acting on the leading edge of keratocytes, which is much less than what we measure as a stall force, can stop protrusion by probably interfering with nascent adhesions [Bohnet et al., 2006]). Also, in vivo, mechanical contact can trigger local mechanochemical pathways that generate signals, causing the delocalization of polymerization-maintaining complexes. Nevertheless, our results provide the first direct measurements of lamellipodial protrusion force characteristics of a crawling cell and, therefore, represent a mechanical benchmark against which the adequacy of our theoretical understanding of protrusion can be judged.

Materials and methods

Cell culture and reagents

Fish keratocytes were cultured from the scales of rainbow trout (*Oncorhynchus mykiss*). The scales were removed from the freshly killed fish and transferred into 100 ml of start medium (17.5 ml RPMI 1640 without phenol red, 14 ml Fish Ringers [0.22 mM NaCl, 4 mM KCl, 4.8 mM $NaHCO_3$, 2 mM $CaCl_2$, and 2 mM Tris], 4 ml FCS, 1.2 ml penicillin/streptomycin, 1 ml of 1 M Hepes, and 1 ml Steinberg medium [0.52 M NaCl, 3 mM $Ca(NO_3)_2$, 6 mM KCl, and 8.6 mM $MgSO_4$]) and washed several times. The scales were then sandwiched between two microscope slides (Menzel-Gläser) with 200 μl of the start medium and left overnight at 4°C. Clusters of cells grew out from the scales, and these were dissociated by treating with EDTA/trypsin for 30 s and washing with 100 ml of running medium (20 ml Fish Ringers, 1 ml Steinberg medium, and 1 ml of 1 M Hepes). Single cells began to migrate after ~5 min. All chemicals were purchased from Sigma-Aldrich or Biochrom. Experiments were usually performed within a few minutes after cells started to migrate. Cells were kept at 4°C until they were transferred to the optical microscopes, which were at room temperature.

Force measurement microscopy

A 200 × 200 × 20-μm piezostage (Physik Instrumente) was integrated into a thick aluminum plate that replaced the stage on an optical microscope (Axiovert 135 TV; Carl Zeiss MicroImaging, Inc.) such that a microscope slide with cells could be micropositioned in x, y, and z (Fig. S1, available at http://www.jcb.org/cgi/content/full/jcb.200601159/DC1). A second thick aluminum plate was placed on top of the Axiovert stage and supported by three adjustable points. An AFM cantilever (microlever obtained from Veeco Instruments) was mounted on a plexiglass holder and inserted in a recess of the second aluminum plate so that the cantilever was oriented perpendicular to the substrate (Fig. 1 a). The spring constant of the cantilevers was measured according to the thermal noise method (Butt and Jaschke, 1995) and was found to be in the range of 7 mN/m. To adjust the distance between the cantilever and microscope slide, the slide was oscillated in the y direction by driving the piezo with a sine function, and the cantilver was lowered so that it was in contact with the slide. Then the cantilever was retracted until its oscillation disappeared. To compensate for potential drift, we retracted the cantilever further by 80–100 nm. This procedure was applied just before each measurement. Cells were positioned in front of the cantilever, and its deflection after cell contact was recorded with a CCD camera (4912-5100/0000; Cohu) and a videocassette recorder (TL300; Panasonic).

RICM

RICM was performed on the same Axiovert 135 TV optical microscope as the force measurement and with the same setup for holding the cantilever. A mercury lamp (HBO 50; Carl Zeiss MicroImaging, Inc.), an antiflex slider, and a 63× antiflex objective together with standard oil immersion objectives (n = 1.518; all components were purchased from Carl Zeiss MicroImaging, Inc.) were used. Cells were prepared on coverslips (Omnilab). The coverslips were attached with magnets to a stainless steel holder to allow free access from the top. In this series of experiments, uncoated cantilevers (MLCT-NONM; Veeco Instruments) were brought in contact with the glass slide and served as fixed obstacles. A green bandpass filter (D535/40; Chroma Technology Corp.) was used to avoid damage of the cells by UV light and to enhance contrast in the RICM image. The sequences were recorded with a 12-bit CCD camera (Retiga 4000R FAST Mono; QImaging) and transferred directly to a computer (MacIntosh G4; Apple) via fire wire.

Fluorescence and AFM

The cells were prepared for fluorescence as described previously (Lee and Jacobson, 1997). In brief, ~500 μl of a mixture of 1.5 ml PBS, 0.5 ml of 0.1% Triton X-100 in PBS, 100 μl of 50% glutaraldehyde in water, and ≤100 μl of 100 μg/ml rhodamine-phalloidin in MeOH was introduced shortly after the lamellipod struck the cantilever. After ~1 min of incubation with the fixation and staining mixture, cells were washed several times in PBS and imaged later with an Axiovert 135 TV microscope. Images were recorded with a Visicam (Visitron Systems) using CamWare 1.26 (PCO AG) and a PC operated with Windows 2000 SP4 (Microsoft). Contact-mode AFM on fixed and stained cells was performed on a microscope (MFP3D; Asylum Research).

Data acquisition and analysis

Force measurements were performed as follows: the recorded video frames were digitized with a frame grabber card (AG-5; Scion Corp.) using ImageJ 1.33u software (National Institutes of Health). The time period of interest (deflection of the cantilever by the lamellipod) was recorded in 768 × 512-pixel images at 25 frames/s. For each image, we averaged five neighboring horizontal lines, which were perpendicular to the cantilever. Because the cantilever is the brightest object in this line, the position of the edge could be defined by looking at a certain gray value. By following this position, we were able to determine the deflection as a function of time. Calibration was performed with a stage micrometer (100 lines per millimeter; Leitz) to generate deflection versus time graphs.

These data sets contained a significant amount of noise and were smoothed by using a spline fit option of IGOR Pro (WaveMetrics). The smoothing factor was set to one, and the SD was varied to obtain the best fit. To produce force-velocity curves, the velocity of the tip was obtained by differentiating the smoothed position versus time curve, whereas the force was calculated from Hooke's Law. Velocity versus force curves were normalized by the initial velocity of the cantilever (v_{max}) and by the force at the point where $v = v_{max}/2$ ($f_{1/2}$). Error bars for the force were calculated by using the SD of the deflection. Errors in velocity were not calculated because the position versus time data had to be smoothed before taking the derivative.

For AFM, height profiles were obtained after flattening height images with a second order flatten option, which is available in the IGOR software. The recording and analysis were performed with IGOR Pro. For RICM, the images were recorded with a 512 × 512-pixel array and an exposure time of 1 s. The position of the adhesions at the front of the lamellipod, as detected by RICM, were recorded from ~30 s before cantilever contact to the last visible position of the leading edge (as a result of the high reflection of the cantilever). Using IGOR Pro, kymographs were constructed from the time series of images (Fig. 4, b and c) by extracting lines from the videos that capture the collision of the leading edge with the cantilever; spatial differentiation of such lines gave sharper edge detection. Calibration was performed with a stage micrometer.

Online supplemental material

Video 1 is a typical video of a trout keratocyte deflecting an AFM cantilever until the cell passes under the cantilever, which then springs back to its initial position. Video 2 is an RICM video showing cell movement before contact with the leading edge of a keratocyte, during initial contact, and during contact with the body of the cell. Fig. S1 is a schematic of the cantilever-positioning stage. Supplemental material provides data on the biophysics of possible force generation mechanisms. Online supplemental material is available at http://www.jcb.org/cgi/content/full/jcb.200601159/DC1.

This work was supported by the National Science Foundation grant DMS-0315782 (to A. Mogilner), the National Institutes of Health Cell Migration Consortium grant GM 64346 (to K. Jacobson, A. Mogilner, and M. Radmacher), and the University of Bremen FNK grant 01/115/04 (to M. Prass and M. Radmacher).

Submitted: 27 January 2006
Accepted: 7 August 2006

References

Abraham, V.C., V. Krishnamurthi, D.L. Taylor, and F. Lanni. 1999. The actin-based nanomachine at the leading edge of migrating cells. *Biophys. J.* 77:1721–1732.

Bohnet, S., R. Ananthakrishnan, A. Mogilner, J.-J. Meister, and A.B. Verkhovsky. 2006. Weak force stalls protrusion at the leading edge of the lamellipodium. *Biophys. J.* 90:1810–1820.

Bray, D. 2001. Cell Movements: from Molecules to Motility. Garland Press, NY. 372 pp.

Butt, H.-J., and M. Jaschke. 1995. Calculation of thermal noise in atomic force microscopy. *Nanotechnology.* 6:1–7.

Carlsson, A. 2003. Growth velocities of branched actin networks. *Biophys. J.* 84:2907–2918.

Charras, G., J. Yarrow, M. Horton, L. Mahadevan, and T. Mitchison. 2005. Non-equilibration of hydrostatic pressure in blebbing cells. *Nature*. 435:365–369.

Condeelis, J. 1993. Life at the leading edge: the formation of cell protrusions. *Annu. Rev. Cell Biol.* 9:411–444.

Dickinson, R., L. Caro, and D. Purich. 2004. Force generation by cytoskeletal filament end-tracking proteins. *Biophys. J.* 87:2838–2854.

Felder, S., and E.L. Elson. 1990. Mechanics of fibroblast locomotion: quantitative analysis of forces and motions at the leading lamellas of fibroblasts. *J. Cell Biol.* 111:2513–2526.

Herant, M., W. Marganski, and M. Dembo. 2003. The mechanics of neutrophils: synthetic modeling of three experiments. *Biophys. J.* 84:3389–3413.

Iwaki, M., H. Tanaka, A.H. Iwane, E. Katayama, M. Ikebe, and T. Yanagida. 2006. Cargo-binding makes a wild-type single-headed myosin-VI move processively. *Biophys. J.* 90:3643–3652.

Jurado, C., J.R. Haserick, and J. Lee. 2005. Slipping or gripping? Fluorescent speckle microscopy in fish keratocytes reveals two different mechanisms for generating a retrograde flow of actin. *Mol. Biol. Cell*. 16:507–518.

Ladam, G., L. Vonna, and E. Sackmann. 2005. Protrusion force transmission of amoeboid cells crawling on soft biological tissue. *Acta Biomater*. 1:485–497.

Lauffenburger, D.A., and A.F. Horwitz. 1996. Cell migration: a physically integrated molecular process. *Cell*. 84:359–369.

Laurent, V., S. Kasas, A. Yersin, T. Schaffer, S. Catsicas, G. Dietler, A. Verkhovsky, and J. Meister. 2005. Gradient of rigidity in the lamellipodia of migrating cells revealed by atomic force microscopy. *Biophys. J.* 89:667–675.

Lee, J., and K. Jacobson. 1997. The composition and dynamics of cell-substratum adhesions in locomoting fish keratocytes. *J. Cell Sci.* 110:2833–2844.

Marcy, Y., J. Prost, M. Carlier, and C. Sykes. 2004. Forces generated during actin-based propulsion: a direct measurement by micromanipulation. *Proc. Natl. Acad. Sci. USA*. 101:5992–5997.

McGrath, J., N. Eungdamrong, C. Fisher, F. Peng, L. Mahadevan, T. Mitchison, and S. Kuo. 2003. The force-velocity relationship for the actin-based motility of *Listeria*. *Curr. Biol.* 13:329–332.

Mogilner, A., and G. Oster. 1996. Cell motility driven by actin polymerization. *Biophys. J.* 71:3030–3045.

Mogilner, A., and G. Oster. 2003. Force generation by actin polymerization II: the elastic ratchet and tethered filaments. *Biophys. J.* 84:1591–1605.

Oliver, T., M. Dembo, and K. Jacobson. 1995. Traction forces in locomoting cells. *Cell Motil. Cytoskeleton*. 31:225–240.

Parekh, S., O. Chaudhuri, J. Theriot, and D. Fletcher. 2005. Loading history determines the velocity of actin-network growth. *Nat. Cell Biol.* 7:1219–1223. (published erratum appears in *Nat. Cell Biol.* 2006. 8:100).

Pollard, T., and G. Borisy. 2003. Cellular motility driven by assembly and disassembly of actin filaments. *Cell*. 112:453–465.

Ridley, A., M.A. Schwartz, K. Burridge, R.A. Firtel, M.H. Ginsberg, G. Borisy, J.T. Parsons, and A.R. Horwitz. 2003. Cell migration: integrating signals from front to back. *Science*. 302:1704–1709.

Schnitzer, M.J., K. Visscher, and S.M. Block. 2000. Force production by single kinesin motors. *Nat. Cell Biol.* 2:718–723.

Small, J., T. Stradal, E. Vignal, and K. Rottner. 2002. The lamellipodium: where motility begins. *Trends Cell Biol.* 12:112–120.

Wang, M.D., M.J. Schnitzer, H. Yin, R. Landick, J. Gelles, and S.M. Block. 1998. Force and velocity measured for single molecules of RNA polymerase. *Science*. 282:902–907.

Wiesner, S., E. Helfer, D. Difry, G. Ducouret, F. Lafuma, M. Carlier, and D. Pantaloni. 2003. A biomimetic motility assay provides insight into the mechanism of actin-based motility. *J. Cell Biol.* 160:387–398.